UNCONVENTIONAL RESOURCES TECHNOLOGY CONFERENCE
FUELED BY SPE • AAPG • SEG

URTeC: 2902355

Microseismicity Analysis for HFTS Pad and Correlation With Completion Parameters

Debotyam Maity*[1]
1. Gas Technology Institute

Abstract

Microseismic data can be used as a tool to help understand fracturing behavior during hydraulic stimulation. Recent studies have validated complex fracture growth and interaction during fracturing process and there is a need to better utilize microseismic data as a way of improving our understanding of this complexity. Moreover, significant stress variations along the laterals and various formations of interest can be better interpreted by making use of b-value distribution as a proxy measure for stress. In this study, we tie the Frequency Magnitude Distributions (FMD) from microseismic with the 3D seismic and petrophysical data to understand stress variations within the upper and middle Wolfcamp formations. We also look at how temporal microseismic FMD variance can be used as a tool to help understand fracturing behavior with time. Our results highlight the utility of microseismic FMD as a valuable hydraulic fracturing diagnostic tool post fracturing operations and as a validation for observations made during treatment including relevant treatment parameters.

Introduction

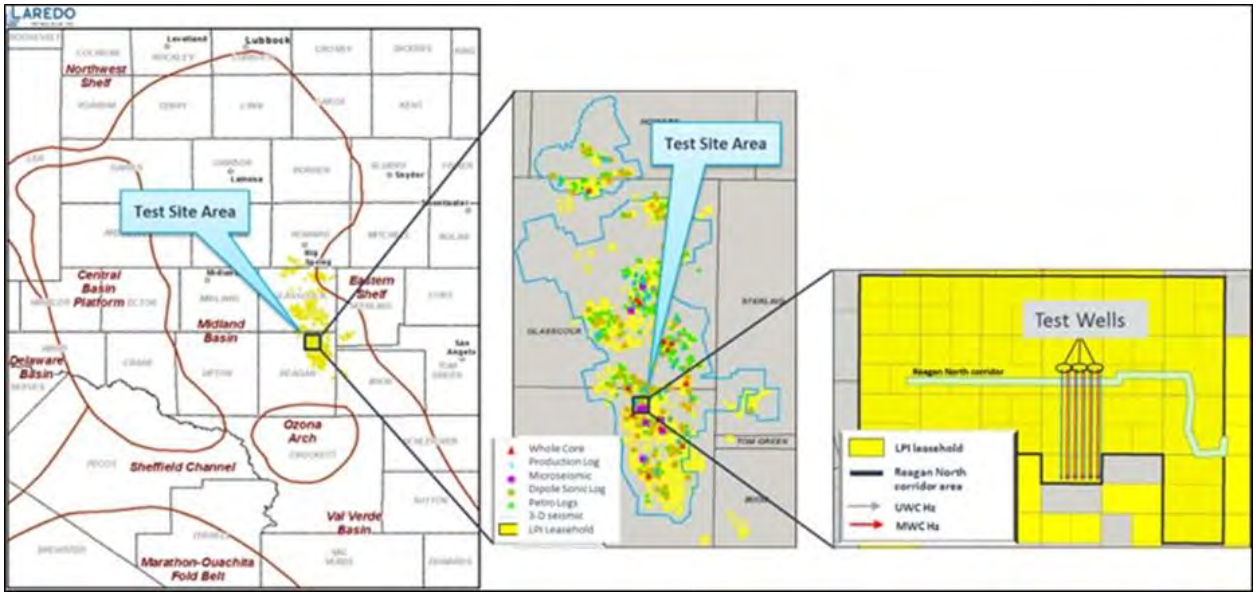

Figure 1: Left panel: Location of the Laredo Petroleum leasehold in reference to the geologic setting of the Midland Basin. Middle Panel: Expanded view of Laredo leasehold, including the location of the HFTS. Right Panel: Orientation and producing formation of the newly drilled 11 test wells from this study.

The Hydraulic Fracturing Test Site (HFTS) is located on the eastern part of the Midland Basin, between the Central Basin Platform and the Eastern Shelf. The test wells are located in Reagan County, Texas and are operated by Laredo Petroleum (Figure 1 left panel). The test site includes a high quality 3-D seismic survey and it is surrounded by many producing wells. There are many wells with open- and cased-hole petrophysical, production and image logs, as wells as whole and sidewall cores. Additionally, microseismic surveys were collected during stimulation of selected wells (Figure 1 right panel). There are a total of 11 new wells drilled in the Upper and Middle Wolfcamp formations as part of this study, with five wells in the Middle Wolfcamp and six in the Upper Wolfcamp. The new wells are all horizontal with extended reach lateral sections (~ 10,000 feet), drilled from north to south, and normal to the predicted maximum horizontal stress orientation.

This study also involved significant data collection efforts including micro Diagnostic Formation Injection Tests (DFIT), advanced open-hole logs, 110 side wall cores, complete core analysis including petrophysics, geomechanical analysis and petrography imaging, tracers, microseismic, tilt-meter surveys, bottom-hole pressure data, multiple pre- and post-treatment cross-well seismic surveys, etc. The microseismic monitoring for HFTS was a comprehensive program involving monitoring operations for almost all of the hydraulically fractured stages (~ 380 stages for 11 well pad main experiment). For a vast majority of the completed stages, a multi-array monitoring approach was utilized involving both a vertical and a sliding horizontal array. The aim was to get the best coverage possible using both the arrays such that the uncertainties in processing could be reduced. The horizontal tool-string was placed in one of the horizontal laterals. The horizontal array had 12 levels made up of 18 geophone sensors. The vertical array had eight levels made up of 16 geophone sensors. Data collection and real-time processing was used for monitoring the treatments over a period of more than 45 days. Overall, the average event density per stage for this experiment was around ~350 and the average moment magnitude was around -2. Based on the high-resolution event catalog available from the processing of available microseismic data, a more in-depth analysis of b-value distributions both in space and in time was carried out for better understanding of variability in observed seismicity and how it relates to the reservoirs in question.

Frequency magnitude distributions (FMD) was first theorized by Guttenberg & Richter in 1944. The Gutenberg-Richter law provides the relation between the magnitude and the total number of earthquakes in any given region and/ or time of at-least that magnitude. It can be defined as:

$$\boldsymbol{N = 10^{a-bM}} \tag{1}$$

Here N is the number of events having a magnitude $\geq M$. Parameters ‘a’ and ‘b’ are constants. The parameter ‘b’ is generally known to be close to ‘1’ for seismically active regions such as the San Andreas Fault which extends about 750 miles through California and forms the tectonic boundary between the North American Plate to the east and the Pacific Plate to the west. The source environment of the region is relevant and influences the range of b values that can be observed. During earthquake swarms, values much higher than ‘2’ are common indicating relative preponderance of smaller earthquakes. The parameter ‘a’ indicates total seismicity rate of a region. At smaller moment magnitudes, a large number of events might remain undetected due to inherent instrumentation and seismic survey design limitations. This generally results in an apparent b-value roll-off at these significantly lower magnitudes. A magnitude cut-off is generally applied and is referred to as the magnitude of completeness (M_C). This is done to limit data such that only magnitudes higher than M_C are used in slope calculations.

The b-value is believed to be an indicator of stress state of the subsurface. In a reservoir where seismicity is induced through injection or production operations, a b-value less than 1 indicates compressive (reverse faulting or fracture closure) regime, a b-value close to 1 indicates shear or slip failure while a b-value higher than 1 indicates tensile or normal faulting regime (Grob & van der Baan, 2012). In short, smaller b-values indicate relatively larger number of bigger microseisms while larger b-values indicate relatively higher number of smaller magnitude events. Laboratory experiments involving acoustic emissions from fracturing rock samples have shown a direct correlation between higher b-values and higher crack densities (Wang et al., 2000). The same study also highlights an inverse correlation with relative size distribution of shorter cracks. In the field of hydraulic fracturing, Vermylen (2011) showed a direct relationship between b-values and instantaneous shut in pressure (ISIP) for individual fracturing stages (Figure 2). This is in line with other teleseismic observations such as by Scholz (2015) since the relationship with differential stress should be inverse. Another recent study showed an inverse relationship for b-value with ISIP’s (Sil et al., 2012). Of-course, ISIP is not a reliable indicator of in-situ min. horizontal stresses due to uncertainties in evaluation as well as stress shadowing artifacts, etc. Given some of these divergent observations based on existing literature, it

was relevant to understand how b-value correlates with the stress state of the reservoir at the HFTS site for both the upper and the middle Wolfcamp formations. When computing the cumulative event counts or histogram bins, care has to be taken to make sure erroneous data does not affect our calculations. Figure 3 shows four examples with representative examples of both good and bad quality data. Relevant factors to keep in mind while evaluating b-value are as follows:

1. Use Maximum Likelihood Method (Fisher, 1950) to calculate the slope. This will be detailed in the Method section.
2. Use events bigger than M_C in evaluation. It can be calculated in various ways with the easiest being the maximum curvature which looks for slope change.
3. Make sure that the dataset being used for evaluation is not too small. For relatively accurate calculations, studies recommend at least 200 to 300 microseisms.
4. A maximum magnitude cut-off can also be sometimes useful. This is particularly true for smaller catalogs.

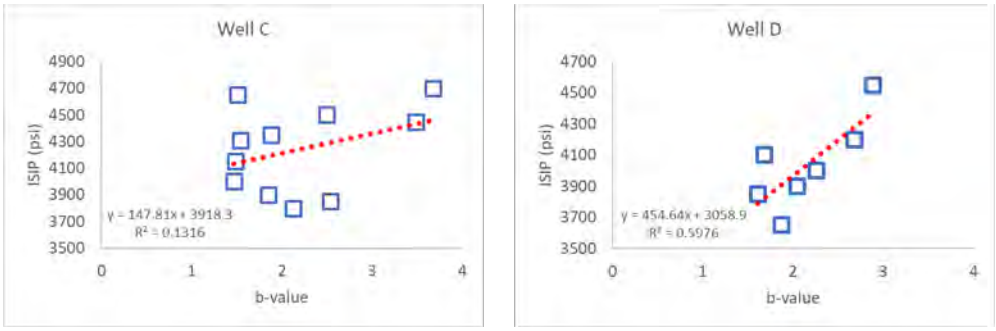

Figure 2: Adapted from Vermylen (2011) plots show relation between ISIP's calculated at pump shut-in vs. b-values calculated for microseismicity recorded for particular stage for two wells.

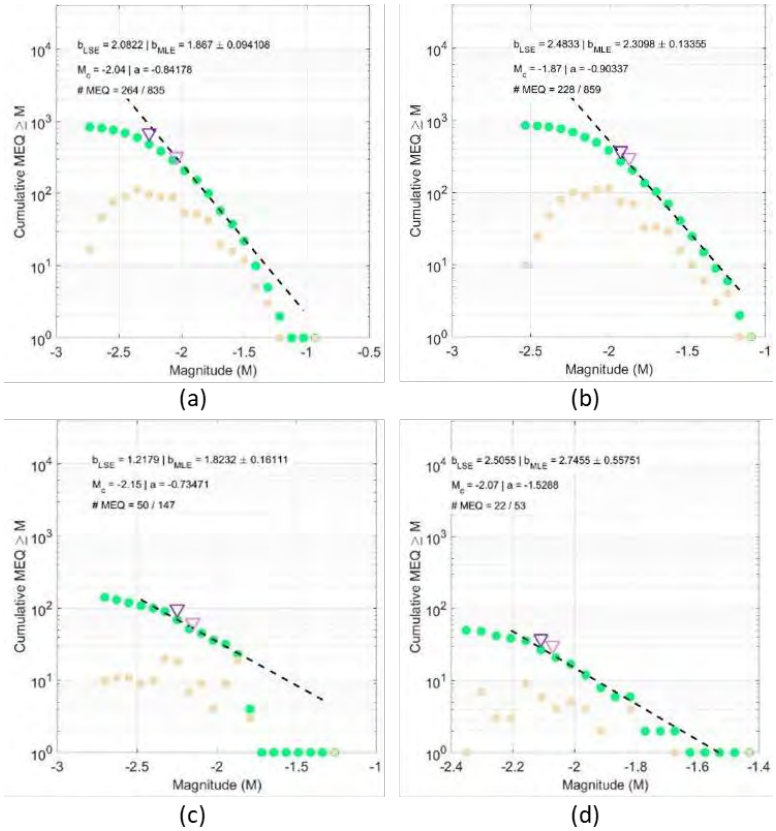

Figure 3: Sample b-value calculations for larger catalogs (subplots a, b) and smaller catalogs (subplots c, d) highlighitng impact of smaller catalogs on uncertainty and accuracy.

In this study, we also look at Ant tracking results from high-resolution 3D seismic data collected at the HFTS study area. Ant tracking (Basir, et al., 2013; Ngeri, et al., 2015) is an Ant Colony Optimization (ACO) approach (Dorigo, 1992) used to enhance detection of discontinuities within the data. It uses swarm intelligence approach, which is based on the collective behavior of ants. Social organisms, such as ants carry out repeated actions such as moving from nesting place to food source and vice versa. Ants secrete pheromones while travelling along these paths. The pheromone trails get used by ants and thus the most efficient (or smallest) paths are actively highlighted compared to less efficient paths. ACO is a frequently used approach in image processing workflows for edge detection and linking tasks.

Method

For the FMD analysis, b-value was computed for the microseismic data for each stage separately as well as based on a 3D gridded reservoir volume. As mentioned before, the maximum likelihood estimate is used to predict the b-value distribution where the M_C is identified using the goodness of fit approach. In this approach, the absolute difference between the observed and synthetic Gutenberg-Richter distribution is minimized. Synthetic distributions are computed using estimated a- and b-values of the observed dataset for all $M \geq M_C$ as a function of ascending M_C. The model fit is found where 90% of the observed data is modeled by a straight line. In case 90% cannot be obtained, the catalog is not analyzed. The maximum likelihood (Fisher, 1950) estimate is given as:

$$\boldsymbol{b_{MLE}} = \frac{\mathbf{1}}{\boldsymbol{ln(10)(\bar{M}-M_C)}} \tag{2}$$

The use of maximum likelihood allows for small variances and relatively smaller changes with addition of newer data, at-least in a statistical sense. The maximum likelihood uncertainty can also be calculated as a standard deviation defined by Shi & Bolt (1982):

$$\boldsymbol{\sigma(b) = 2.3b^2}\sqrt{\frac{\sum_{i=1}^{N}(M_i-\bar{M})^2}{N(N-1)}} \tag{3}$$

Here, $\bar{M}$ denotes the mean moment magnitude of the catalog, M_i denotes the individual magnitudes within the distribution. N is the total size of the catalog and M_C is the cut-off magnitude. For the higher magnitude cut-off threshold, we find the best fit with standard minimized error (L2-norm).

Unlike stage wise b-value calculation, where the observed microseisms captured during treatment of said stage is used for getting the required estimate; for 3D b-value distribution, a grid search approach is used. The lateral separation for said grid was decided at 200 feet while the vertical separation for the grids was decided at 400 feet. The choice of grid spacing is defined by the kind of data density we have available within the study area with the idea being having adequate event populations within each grid for relatively accurate b-value estimates and lower estimate uncertainties.

When it comes to processing 3D seismic data for faults and fractures, usually some frequency filter is applied to extract the higher frequencies. Different frequency response of same fault varies and the same holds true for the same frequency response to faults of varying sizes. For ant-tracks using variance input, we use variance attribute. Variance is an edge method to measure the similarity or coherency of waveforms or traces within lateral or vertical windows. It is useful in mapping discontinuities in seismic data related to faulting and stratigraphy. It is useful in delineating faults, large fractures, channel edges, other unconformities, sequence boundaries, etc. Generally, edge-detection and edge-enhancement methods are applied before variance and/ or chaos calculation and subsequent ant tracking. Chaos is a measure of lack of organization in dip and azimuth estimation. It can be used to detect chaotic structures within seismic data thus highlighting positions of reflector disruptions. Geologically, it can be used to distinguish sediment facies, fault zones, angular unconformities, channel bodies and possible zones of fractures.

Results

Stage wise FMD analysis has revealed a reasonably strong positive correlation between b-value distribution and the estimated ISIP. Table 1 provides the goodness of linear fit for various upper and middle Wolfcamp wells from the study area. For these two formations that are believed to be in a normal faulting stress regime, this indicates an

inverse relationship for b-value distribution with the maximum differential stress. This correlates with that has been observed at various local and teleseismic scales. It should be noted that ISIP is not a very accurate estimate for in-situ minimum horizontal stress and normally only sets a good upper limit for its value. Issues such as stress shadowing add to additional uncertainty apart from issues of accuracy and subjectivity. Still we do observe a positive correlation that extends for all of the wells studied. Another aspect noticed was that for many of these wells, some of the biggest outliers were along the toe side stages. This makes intuitive sense since in an ideal scenario, these stages should have the most significant impact on in-situ stress due to stress shadow effect from one stage to the next and the effect should stabilize after the first few stages. However, removing of the first few stages does not really resolve the issue since the behavior of stress shadow and its impact from one stage to the next is also a function of fracture spacing design as well as in-situ stress conditions. In terms of understanding some of these factors affecting degree of correlation of identified b-value distribution with ISIP, we find that the observed regression fit is inversely correlated with the identified uncertainty in the calculated b-values. On the other hand, there is a direct correlation between the catalog sizes for the stage against the regression fit. This behavior is captured in Figure 4.

Table 1: Ordinary and adjusted coefficients of determination for the b-value vs. ISIP data for stages from multiple UWC and MWC wells.

UWC	Well 2	Well 3	Well 4	Well 5	Well 6
R_o^2	*0.39*	*0.18*	*0.18*	*0.12*	*0.31*
R_a^2	*0.37*	*0.15*	*0.14*	*0.06*	*0.26*
MWC	**Well 7**	**Well 8**	**Well 9**	**Well 10**	**Well 11**
R_o^2	*0.76*	*0.72*	*0.25*	*0.27*	*0.44*
R_a^2	*0.73*	*0.69*	*0.24*	*0.25*	*0.41*

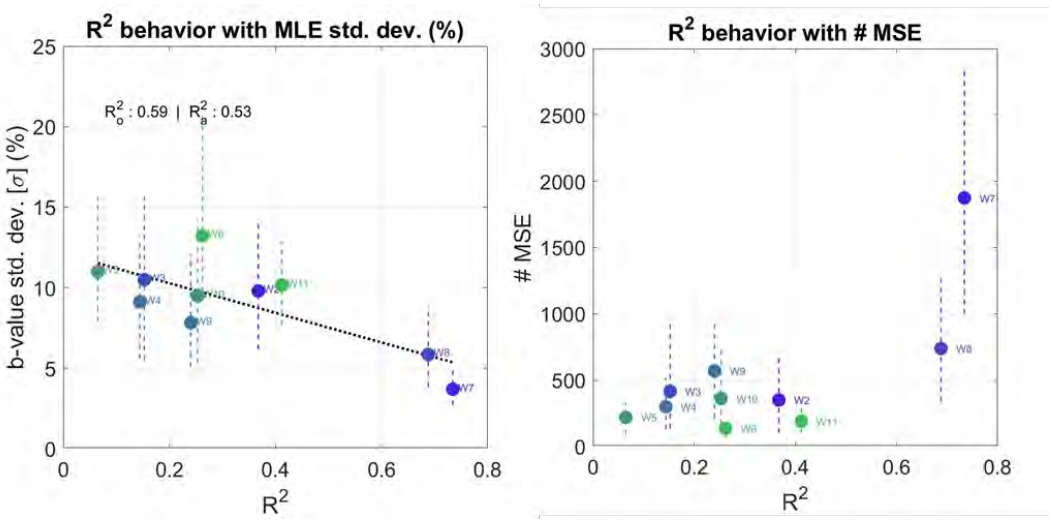

Figure 4: ISIP vs. b-value regression fit R^2's compared with FMD evaluation uncertainty (left) and catalog size (right). Note that the wells with the best linear fit have the lowest errors and largest catalog sizes on average.

This helps us understand how the correlation between identified stage wise b-value distribution and ISIP values relate to the uncertainty in the estimated b-values as well as the total number of microseismic events associated with each well. We also note that for wells W7 & W8 that show the best correlation, the data was only available for the heel end of the laterals to begin with due to lack of geophone coverage. The vertical bars for each point represents the range of values observed while the value at the marker is the mean of the distribution. It is important that any FMD analysis involving local seismicity should have adequate microseismic event count as higher event counts lead to lower uncertainties in evaluated values. Using M_C or total event count on their own may not provide a good measure of usability of a given seismic catalog though. In this study, a minimum requirement was set at 300

microseismic events and a calculated mean standard deviation for the catalogs was set at less than 15%. For a b-value of '2', this translates to uncertainty band of ± 0.3.

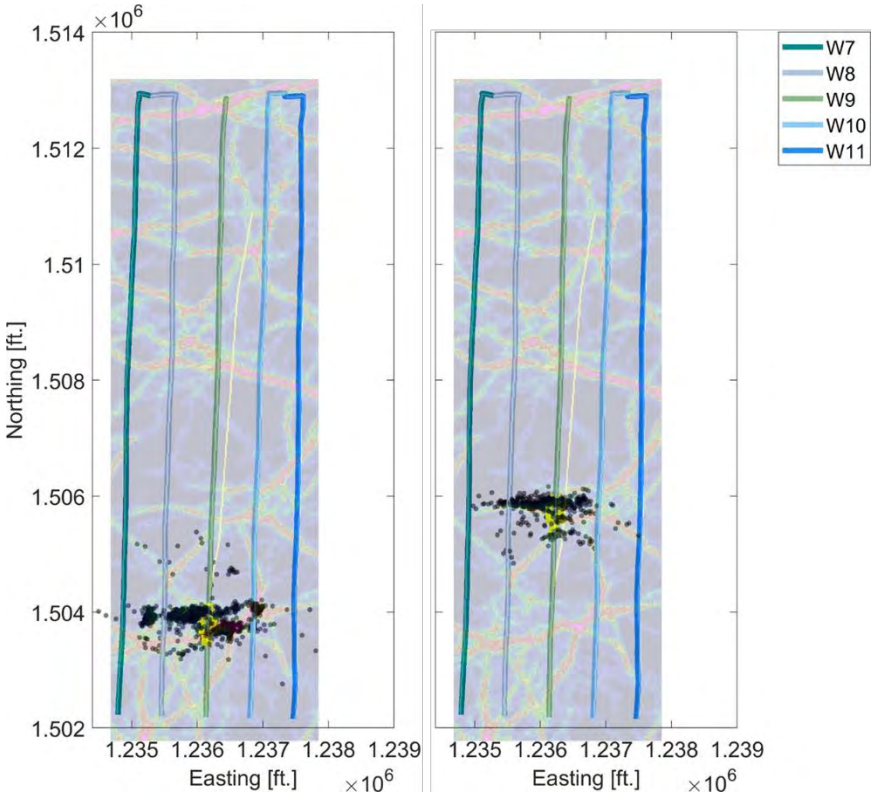

Figure 5: Observed seismicity for two reference stages superimposed on seismic derived ant track map at relevant depth. The seismicity distribution highlights the potential impact of local geologic heterogeneities on hydraulic fracturing.

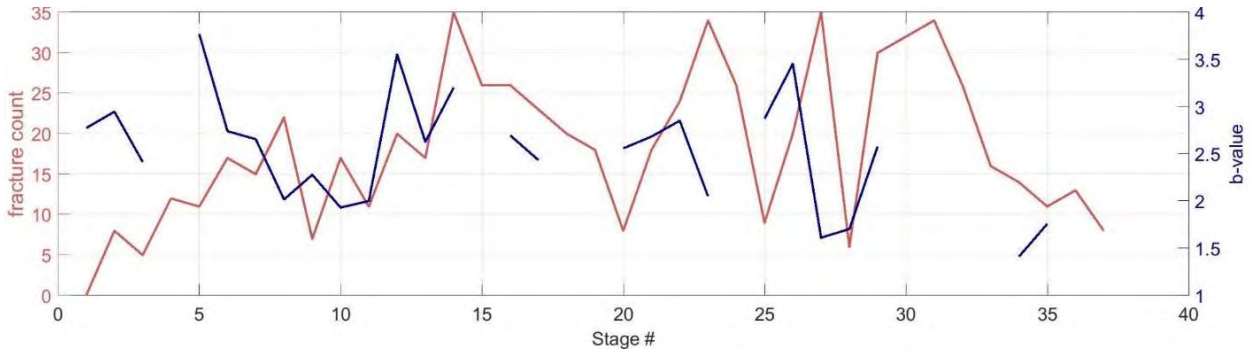

Figure 6: OBMI derived fracture density (counts per stage based on completion design) compared with the calculated b-values. Notice similar trend behavior but evidence of offsetting towards the heel of the well.

We understand that with hydraulic fracturing, the seismicity is significantly influenced by local heterogeneities. The seismic ant track volumes provide a good indication of possible local faults, fracture swarms or debris flows. Figure 5 shows the microseismic events from two reference stages. The complexity can easily be correlated with the observed lineaments from the ant track volume extracted at the same depths of interest. Another way to identify the influence of local heterogeneities is to look at the OBMI image logs and how the local or near wellbore fracture distribution as observed from the image logs correlate with the calculated stage wise b-values. Figure 6 shows an example comparing b-values with the fracture density. It is interesting that while we can clearly see some degree of correlation between the two data trends, there is some evidence of offsetting behavior that could be due to connected fracture/ fault systems pushing the seismicity away from the treatment stage laterally to another portion upstream or

downstream along the well. To understand the relation between observed lineaments from the seismic derived ant tracks and the FMD b-values, a 3D distribution of b-value within the reservoir of interest was calculated. To make sure that the calculated values were reasonably accurate, a cut-off of 100 events was used and for any grid with less events, a reference value of '0' was set since that holds no physical meaning.

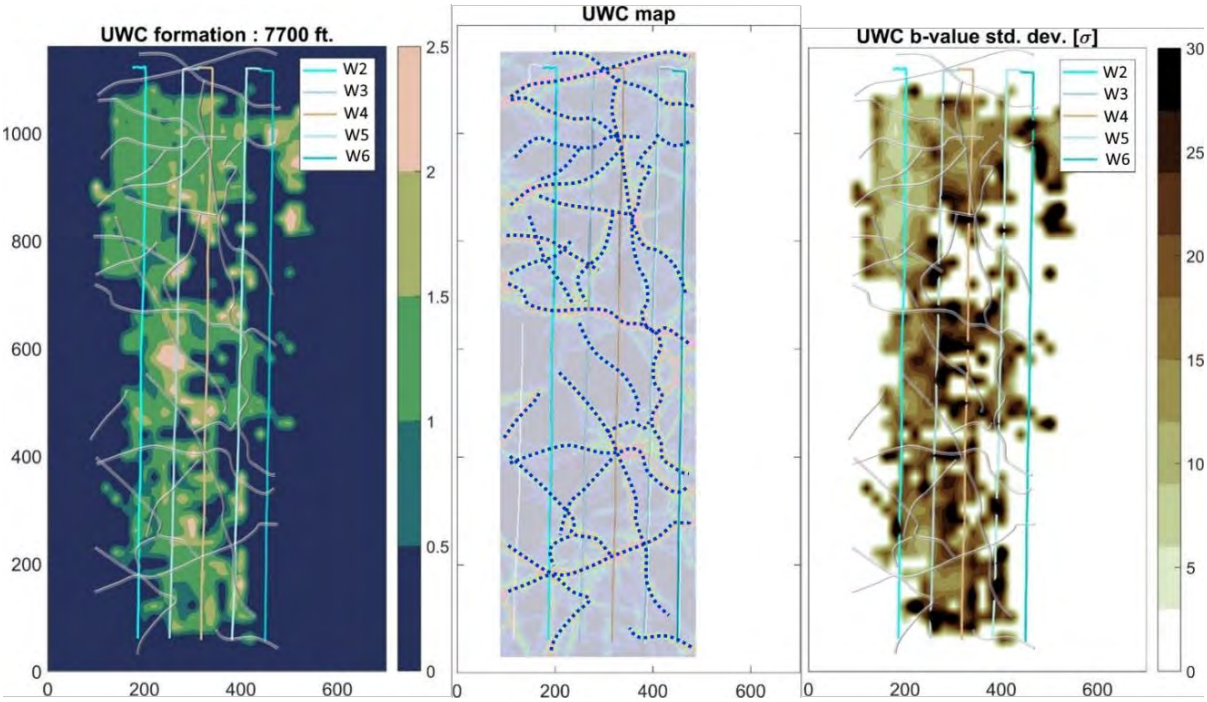

Figure 7: 3D distribution of b-value and associated uncertainty across the upper Wolfcamp wells. The ant track lineaments from 3D seismic are superimposed for reference.

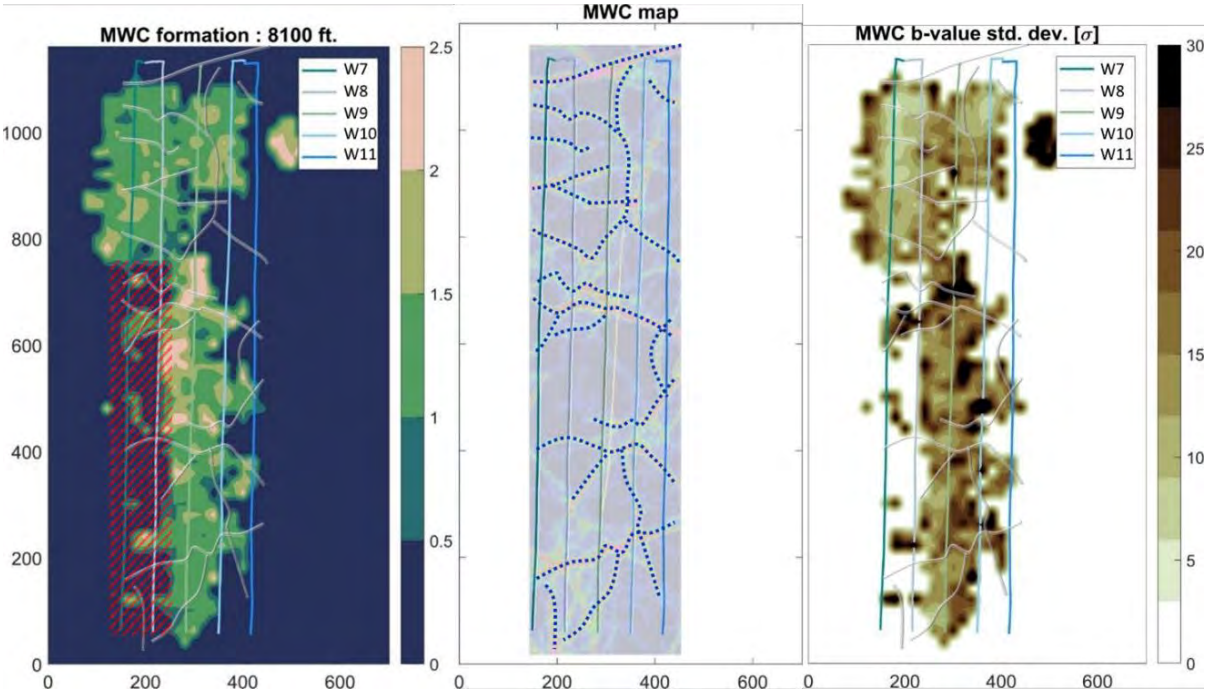

Figure 8: 3D distribution of b-value and associated uncertainty across the middle Wolfcamp wells. The ant track lineaments from 3D seismic are superimposed for reference. The red hatched zone represents general location of fracture stages with no microseismic coverage.

Figure 7 and Figure 8 show the identified distributions along with the standard deviations from this grid search. The lineaments on top of these map views are prominent lineaments that have been extracted from the 3D seismic ant tracks from depths associated with the corresponding formations. Careful examination of b-value behavior close to the identified lineaments shows us that lineaments seem to align with regionally low b-value trends. High b-value trends seem to show up in areas bordering the identified lineaments, in areas with little to no lineaments or in areas where there seems to be a significant confluence of multiple lineaments. To highlight this behavior, we extract the values along one of the treatment wells (W9). Figure 10 shows the b-value distribution across this well as well as the location of the lineaments highlighted using the red inserts. Barring few exceptions, most locations with lineaments correlate with low microseismic derived "b-value". Since the values are higher than '1' in almost all cases, the failure of associated seismicity should be mostly tensile. However, if we consider the lineaments to include significant population of preexisting planes of weakness, there should be more shear activation associated with those regions. Fracture density drops with distance from faults (damage zone fracture mechanics) thus leading to lower values at discontinuities and higher values (increased occurrence of tensile failure) away from discontinuities.

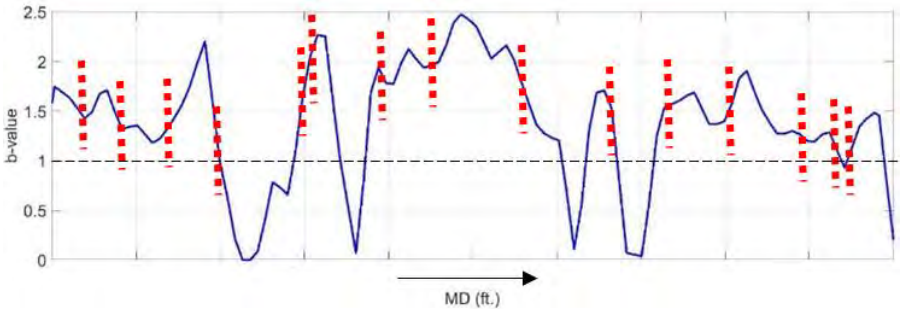

Figure 10: Influence of observed lineaments on seismicity for a reference well. Red inserts show location of lineaments as identified from Ant Track valume from 3D seismic data interpretation.

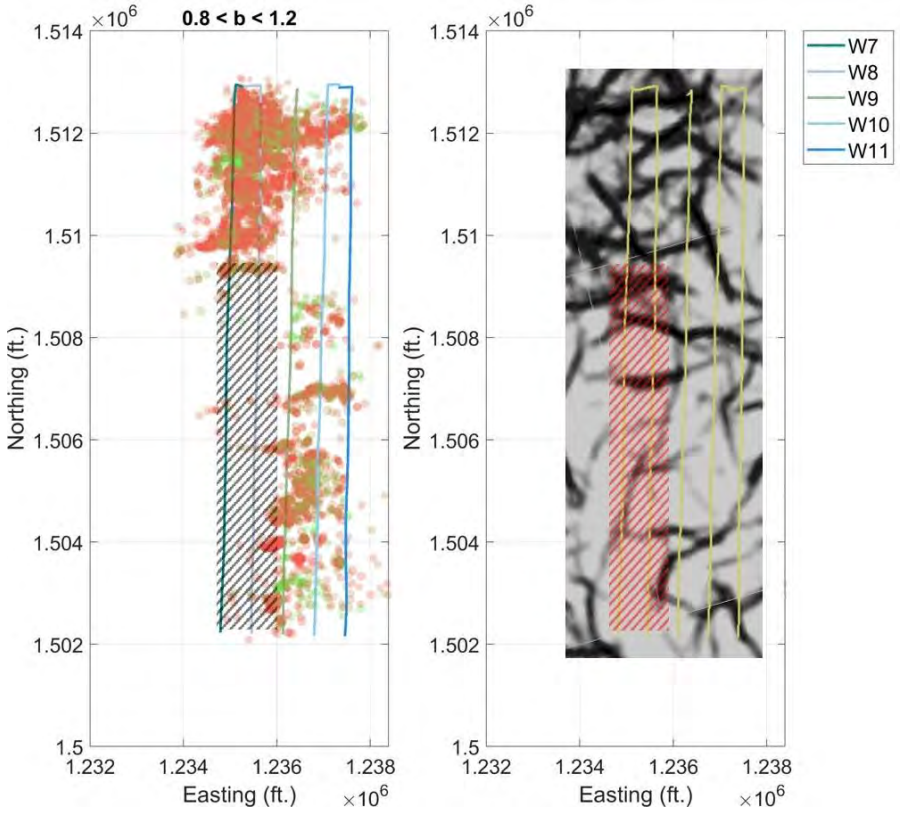

Figure 9: Observed microseismicity within ±100 feet of the MWC wells which fall within b-value close to 1 (left) and Ant Track derived discontinuity attribute (chaos) within 100 feet of the MWC well landing zones (right). Hatched zone highlights broad location of stages with no microsismic coverage.

Next, we try to understand how this behavior affects or relates to the stress state of different sections of the reservoir. As discussed, the identified correlation between lineaments and reduced b-value distribution could be indicative of higher degree of shear activations and failures. From a geomechanical perspective, this could indicate lower minimum horizontal stresses of bigger faults and fractures. Usually, it is believed that clastic rocks have a higher fracture density than carbonates but cracks in carbonates tend to be larger. Thus, b-values should be higher in clastic rocks than in carbonates. This would also indicate that some of those lineaments could be carbonate debris flows within the reservoir and could potentially act as frac barriers. For further validation, we look at the distribution of seismicity which fall within a narrow b-value band (0.8 to 1.2) as those are most likely associated with shear failure along bigger faults/ fractures. Figure 9 shows the microseismicity distribution for the middle Wolfcamp wells as well as the Ant Track chaos attribute at the depth of interest. The attribute was summed over a depth interval of 100 ft. (i.e., the same depth range for which the microseismic event distribution is shown). We can clearly see a significant section towards the heel of the wells in the pad (north end) where the lineaments are very dense and numerous. Towards the middle and the toe end, the lineaments are not that dense and are few in number. The microseismicity distribution as observed during treatment seems to follow the predicted behavior with more events within the range of interest towards the heel and very few events towards the toe end of the pad. While this could be attributed to the lack of microseismic data for a portion of the west wells, the same behavior is observed with the UWC wells where data is available for all of the treated stages.

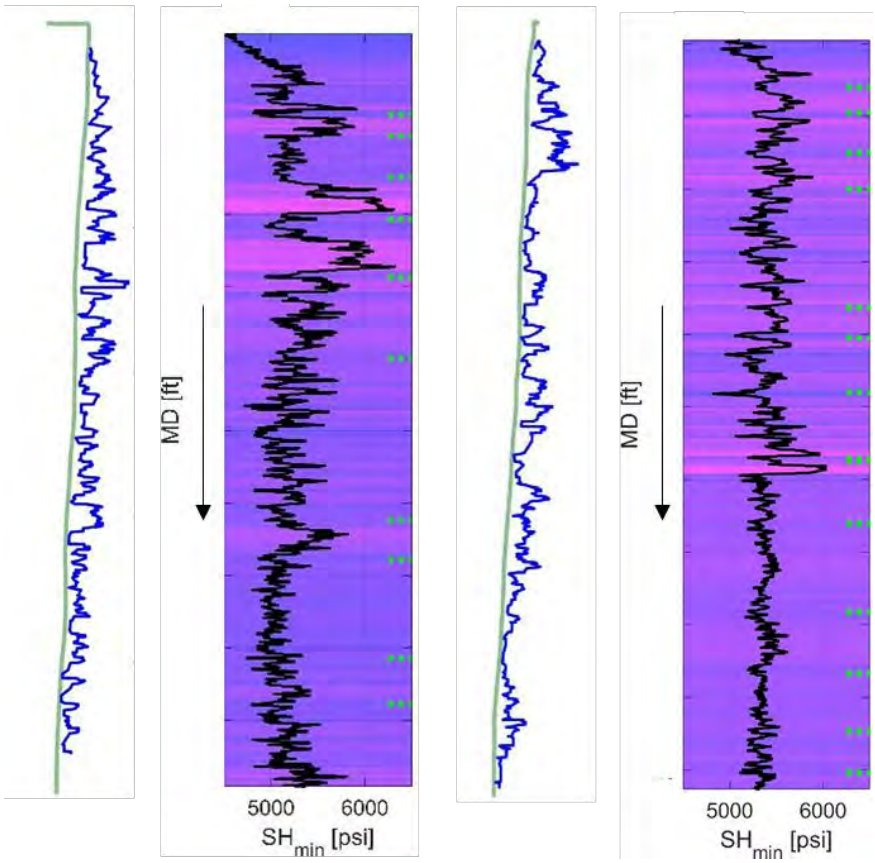

Figure 11: OBMI derived fracture density (blue line curves) compared with modeled minimum horizontal stress (black line curves with variable density map) along two well laterals. The green inserts in the stress plots hilight locations of lineaments.

Next, we look at stress variations along the wellbore lateral based on dipole sonic logs. Anisotropy due to fractures as well as unbalanced formation stresses cause distortion around the borehole that results in shear wave splitting. The azimuth of fast shear waves parallels direction of maximum horizontal stress and azimuth of slow shear wave parallels direction of minimum horizontal stress. Figure 11 shows the modeled minimum horizontal stress for two wells from the test site. The figure also shows the fracture density calculated from OBMI logs along the length of these two laterals in the left panels. We observe significant stress variations towards the heel side halves of these wells compared to the tow ends. These variations could be indicative of more faulting or compartmentalization

within the reservoir compared to the toe side. The lineaments from 3D seismic coincide with boundaries between higher stress and lower stress zones. These high stress zones also coincide in many cases with zones having low fracture density based on OBMI logs.

While until this point, we have discussed b-value analysis from spatial distribution, FMD can also be computed in time with the assumption that all of the seismicity within a specified time window is associated with the same geologic system such as a fracture swarm or clay rich rock, etc. This assumption is necessary if interpretations are to be made that tie the observations from b-value analysis with fracturing/ faulting mechanisms. The key is to look for significant departures from the normal, which can be indicative of significant changes in the fracturing behavior and can help us conduct diagnostics or improve our understanding of effectiveness of hydraulic fracturing operations. Figure 12 shows two examples of time variant FMD behavior for two reference hydraulic fracturing stages. Plots at the bottom for each case highlights the treatment parameters for the said fracturing operations.

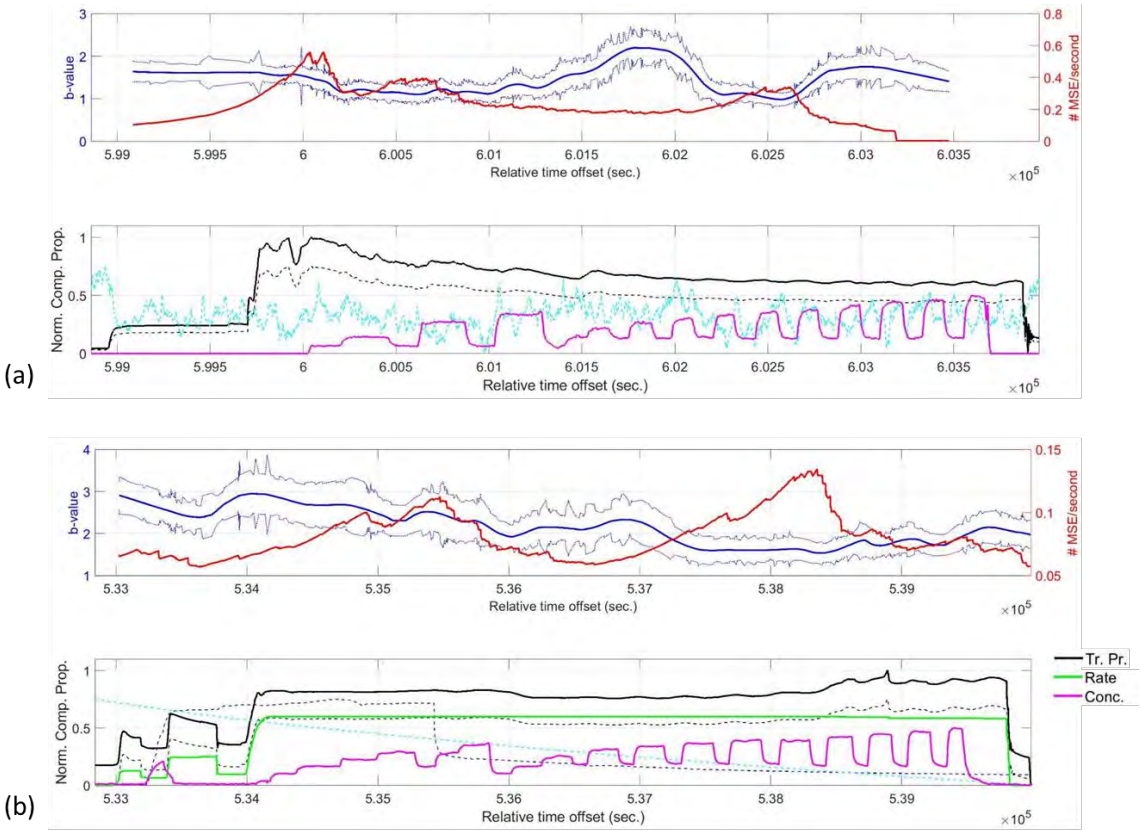

Figure 12: Two example stage data with (a) & (b) from two different stages. The second and the fourth plot are treatment parameters associated with hydraulic fracturing of said stages.

From the first example, we see a slow increase in the b-value once the 40/ 70-mesh proppant starts getting into the formation. The value stays above '2' but then starts to drop back to '1'. It stays low but again jumps towards the end of the treatment. For the second example, the b-value in the beginning is high but during the treatment it drops down to progressively lower values but still stays significantly higher than '1'. We can also see that this apparent b-value behavior seems to be independent of the overall microseismic event density identified in the plots using red curves.

Discussion on potential issues

It is pertinent that we discuss the potential pitfalls in our analysis. The uncertainty associated with b-value analysis is impacted not just by the catalog size and distribution but also the overall catalog quality. Recent studies have also argued on the use of correct moments for magnitude prediction and its impact on b-value calculations and behavior (Jiao et al., 2014). Others have shown that the b-value estimation variances increase with decreasing number of

events in the catalog (e.g., for far-out stages from geophones or those with more severe distance-magnitude thresholding). Increasing bias has also been observed for stages affected with distance-magnitude thresholds (Grob and van der Baan, 2016). For the spatial b-value analysis in this study, uncertainty associated with the processing algorithms for moment magnitudes as well as hypocentral locations are carried forward. Time to depth migration is critical and there might be some error associated with that (velocity model). Getting good overall seismic ties using careful calibration with well logs is critical and so is the need for good well control. We have already discussed the potential uncertainty associated with ISIP estimates since these are broad estimates based on shut-in behavior and may be influenced by local variations in in-situ stress as well as fracturing related artifacts. With the shared analysis, we have compared the lateral variability in b-value behavior. However, variability with depth should also be looked into. This is particularly true since comparison with seismic derived attributes brings along issues of scale and resolution. Properties at seismic scale vary significantly with depth and can cause unrealistic artifacts leading to faulty comparisons.

Conclusions

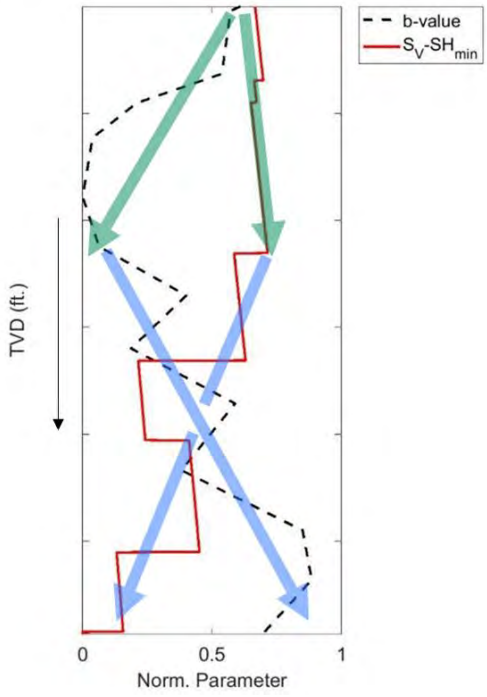

Figure 13: Differential stress and b-value variation with depth at the pilot well within HFTS study area.

Our analysis from the microseismicity observed at the HFTS pad suggests that microseismic b-value is correlated with in-situ stress as well as degree of natural fracturing/ faulting in the subsurface. We have also validated that relatively bigger fractures/ faults or damage zones such as carbonate debris flows can cause lower b-values. This is because longer fractures tend to have larger displacements (if they fail in shear) when compared to smaller fractures, thus causing higher moment magnitudes. Other parameters of interest include degree of cementation, variation in elastic properties, fracture dip/ strike, etc. to name a few. At the HFTS site, ant track lineaments seem to have a correlation with the observed seismicity FMD. This can be reconciled with their interpretation as faults, big fracture swarms, or as debris flows. We note that other geologic explanations could also be plausible in terms of said observations. Based on the observed ISIP from the treatment pressures, we observe a positive correlation of the same with stage wise b-value distributions. This was based on available completion data for 100's of stages from the HFTS site. This observation ties with expected inverse relationship between b-value and maximum differential stress. Figure 13 shows the variations in b-value with depth compared with the differential stress. The stress model assumes hydrostatic pore pressure and a coefficient of internal friction for the rock to be 0.6. The maximum horizontal stress is bounded using frictional faulting theory and wellbore observations. The minimum horizontal stress is constrained using information from DFIT, etc. From the figure, we can clearly see an inverse relationship between the calculated b-value variation with depth and the maximum differential in-situ stress. Note that for b-

value calculation; only microseismic events located laterally within 2000 ft. at any depth interval of the pilot well from the study area were used. This was because many of the stress related observations from sidewall core analysis, logs, etc. came from the pilot well and that in-turn was used to constrain the stresses. The depth window used here for calculation was ±25 feet. We also see how seismic b-value variations mapped in time can be used as a useful indicator of fracturing/ reservoir behavior during completion. It can provide insights regarding nature of seismicity, fracturing or stress state changes with time. All of this is of course contingent upon having adequate microseismic catalog size and quality as well as detection of significantly high number of microseismic events for each stage.

Acknowledgement

We would like to thank the HFTS consortium members for providing guidance in completing this work. We would also like to acknowledge Laredo Petroleum for hosting the test site and providing access to 3D seismic data as well as ant-track seismic volumes. Finally, we would like to thank DOE and NETL for their continued support for the GTI test site program.

References

1. Gutenberg, R. and C. F. Richter (1944). Frequency of earthquakes in California, Bull. Seismol. Soc. Am., 34, 185-188.
2. Grob, M. and M. Van der Baan (2012). Statistical analysis of microseismic event characteristics helps monitor in-situ stress changes. 21st Canadian Rock Mechanics Symposium, RockEng 2012, Edmonton, paper 7058.
3. Wang, Y., X. C. Yin, F. J. Ke, M. F. Xia and K. Y. Peng (2000). Numerical simulation of rock failure and earthquake process on mesoscopic scale. Pure Appl. Geophys., 157, 1905. https://doi.org/10.1007/PL00001067
4. Vermylen, J. and M. D. Zoback (2011). Hydraulic fracturing, microseismic magnitudes, and stress evolution in the Barnett Shale, Texas, USA. SPE Hydraulic Fracturing Technology Conference, The Woodlands, TX.
5. Scholz, C. H. (2015). On the stress dependence of the earthquake b value. Geophys. Res. Lett., 42(5), 1399-1402.
6. Sil, S., B. Bankhead, C. Zhou, and A. Sena (2012). Analysis of B value from Barnett Shale microseismic data. 74th Annual International Conference and Exhibition, EAGE, Extended Abstracts, P094.
7. Fisher, R. A. (1950). Contributions to mathematical statistics. New York: Wiley.
8. Basir, H. M., A. Javaherian, and M. T. Yaraki (2013). Multi-attribute ant-tracking and neural network for fault detection: a case study of an Iranian oilfield, J. Geophys. Eng., 10(1), 015009.
9. Ngeri, A. P., I. Tamunobereton-ari, and A. R. C. Amakiri (2015). Ant-tracker attributes: An effective approach to enhancing fault identification and interpretation, IOSR-JVSP, 5(6), 67-73.
10. Dorigo, M. (1992). Optimization, Learning and Natural Algorithms. Ph.D. Thesis, Politecnico di Milano, Italian.
11. Shi, Y. and B. A. Bolt (1982). The standard error of the magnitude-frequency b value, Bull. Seismol. Soc. Am., 72(5), 1677-1687.
12. Jiao, W., M. Davidson, A. Sena, B. L. Bankhead, Y. Xia, S. Sil, and C. Zhou (2014). The matter of size: On the moment magnitude of microseismic events, Geophysics, 79(3), KS31-KS41.
13. Grob, M. and M. Van der Baan (2016). Influence of acquisition geometry on event cloud asymmetry and on b-value analysis, CSEG Recorder, 41(5), 30-35.